ACS APPLIED MATERIALS & INTERFACES

www.acsami.org

Research Article

Multi-Inlet Spheroid Generator for High-Throughput Combinatorial Drug Screening Based on the Tumor Microenvironment

Seokgyu Han, Sein Kim, Hye Kyung Hong, Yong Beom Cho, Hyo Eun Moon, Sun Ha Paek,* and Sungsu Park*

Cite This: https://doi.org/10.1021/acsami.3c02439

Read Online

ACCESS | Metrics & More | Article Recommendations | Supporting Information

ABSTRACT: Tumor spheroids are powerful tools for drug screening and understanding tumor physiology. Among spheroid formation methods, the hanging drop method is considered most suitable for high-throughput screening (HTS) of anticancer drugs because it does not require surface treatment. However, it still needs to increase the liquid-holding capacity because hanging drops often fall due to the increased pressure caused by the addition of drugs, cells, etc. Here, we report a multi-inlet spheroid generator (MSG) enabling the stable addition of liquid-containing drugs or cells into a spheroid through its side inlet. The MSG was able to load additional solutions through the side inlet without increasing the force applied to the hanging drop. The volume of the additional liquid was easily controlled by varying the diameter of the side inlet. Furthermore, the sequences of the solution injections were manipulated using multiple side inlets. The feasibility of the MSG in clinical application was demonstrated by testing the efficacy of drugs in patient-derived cancer (PDC) cells and controlling the stromal cell ratio in the tumor microenvironment (TME) containing spheroids. Our results suggest that the MSG is a versatile platform for HTS of anticancer drugs and recapitulating the TME.

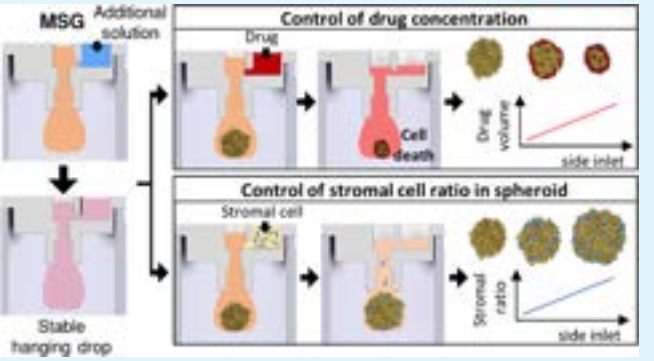

KEYWORDS: *hanging drop, tumor spheroid, drug screening, multi-inlet, volume control*

1. INTRODUCTION

Two-dimensional (2D) cell culture of tumor cells often fails to predict the drug response in cancer patients.[1] This is because this 2D tumor model does not reflect the tumor microenvironment (TME) *in vivo*, in which tumor cells grow three-dimensionally (3D) and interact with stromal and immune cells.[2] Thus, 3D tumor models have emerged as a breakthrough in conventional drug screening[3] because they mimic the TME better than 2D tumor models by forming the 3D structure of tumor cells like spheroids. Tumor spheroids resemble the 3D shape of tumors and constitute the hypoxic core where the tumor cell stemness is enhanced.[4]

Tumor spheroids can be constructed with or without scaffolds.[5] Nonadherent microwells[6] and microfluidics[7] are methods requiring a scaffold that induces spheroid formation and maintains the uniform size of spheroids. Despite these advantages, most of their scaffolds are fabricated only by expensive photolithography or contain complex structures unsuitable for mass production.[8] Spinning flask[9] and hanging drop[10] are methods that do not require a scaffold for constructing 3D tumor spheroid models. Among these scaffold-free methods, the hanging drop method is considered the most suitable for high-throughput screening (HTS) of anticancer drugs because it forms spheroids by aggregating cells in hanging drops without any electrical devices.[11] However, they are still labor-intensive and have limitations in controlling the spheroid size.[12] To solve these problems, recent efforts have been focused on automating the spheroid formation process and improving the spheroid size control.[13] Zhao et al.[14] reported developing a 3D printed hanging drop dripper that generates uniform spheroids in a simple and reproducible manner. However, because it could only hold a few microliters of liquid, it needs to include the cumbersome step of draining some of the media before loading additional liquid-containing drugs or stromal cells. Otherwise, when additional liquid is loaded, direct pressure would be applied to a drop containing a spheroid in the dripper, causing the drop to fall off. This makes it difficult to process large amounts of drugs or add additional cells such as stromal cells for HTS of drug and recapitulating the TME.

Received: February 20, 2023
Accepted: May 15, 2023

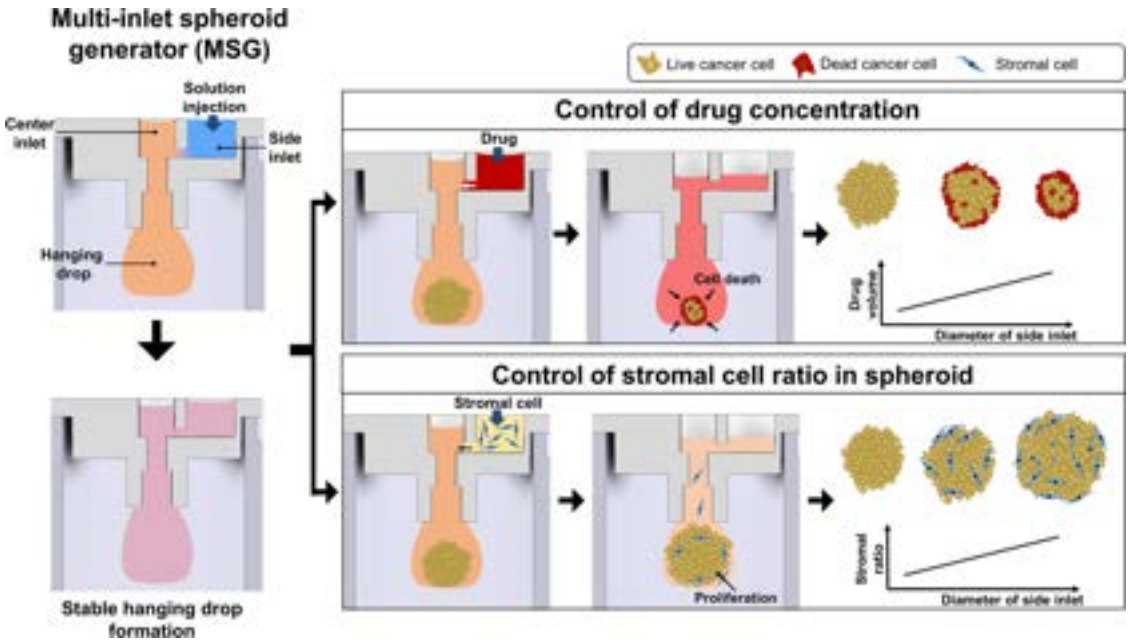

Figure 1. Schematic describing the relative ease of drug testing, and tumor microenvironment (TME) construction by the multi-inlet spheroid generator (MSG) through the formation of stable hanging drops. When tumor spheroids are formed by aggregation of tumor cells injected through the center inlets, different volumes of drugs or stromal cells can be incorporated into spheroids through different diameters of the side inlets.

Several cell culture methods have been developed for HTS of anticancer drugs. These methods include multiwell screening in 3D hydrogel culture,[15] microfluidic chip,[16] and organoid/patient-derived cell culture.[17] In 3D hydrogel culture, cells are encapsulated in a hydrogel, allowing the simulation of the diffusion of in vivo tissues. However, this method can be complex and time-consuming.[18] Microfluidic chip-based methods can reduce consumption and costs by requiring only small amounts of fluids, but they can be challenging for unskilled researchers due to their fabrication complexity and operational limitations. Organoids and patient-derived cells are the best options for mimicking the in vivo system, but they are expensive to culture and can be difficult to analyze due to their various sizes and shapes.

Here, we report a multi-inlet spheroid generator (MSG) that modulates the tumor−stroma ratio (TSR) and drug concentration in a spheroid in an easy and stably controlled manner (Figure 1). The MSG consists of a center inlet connected with a side inlet. The center inlet generates a hanging drop to form a tumor spheroid, while the side inlets are used to load additional liquid-containing drugs or stromal cells into the spheroid. The MSG can hold a larger volume of liquid than the conventional single-inlet spheroid generator (SSG) because unlike the SSG, the MSG can load an additional solution through the side inlet without increasing the force applied to the hanging drop pressure. This was verified by computational fluid dynamics (CFD) simulation. Also, by changing the diameter of side inlets, the volume can be easily controlled. The feasibility of the MSG in clinical application was demonstrated by testing the efficacy of drugs in patient-derived cancer (PDC) cells and controlling the stromal cell ratio in the tumor microenvironment (TME) containing spheroids.

2. MATERIALS AND METHODS

2.1. Materials. Methylcellulose, bovine serum albumin (BSA), agarose, dimethyl sulfoxide (DMSO), temozolomide (TMZ), cisplatin (CDDP), and ethylenediaminetetraacetic acid (EDTA) were purchased from Sigma-Aldrich (St. Louis, MO). Nimustine hydrochloride (ACNU) was purchased from MedChemExpress (Monmouth Junction, NJ). Minimum essential medium (MEM), MEM/F12, penicillin, and streptomycin were purchased from Life Technologies (Carlsbad, CA). Dulbecco's modified Eagle's medium (DMEM) and fetal bovine serum (FBS) were purchased from HyClone Laboratories (Logan, UT). LIVE/DEAD Viability/Cytotoxicity Kit was purchased from Molecular Probes (Eugene, OR). EZ-cytox Cell Viability Assay Kit was purchased from Daeillab Service (Seoul, Korea). Anti-Ki-67 rabbit monoclonal antibody was purchased from Novus Biologicals (Centennial, CO). Blocking solution, horseradish peroxidase (HRP)-labeled polymer-conjugated secondary antibodies against rabbit IgG, Mayer's hematoxylin, and ready-to-use 3,3′-diaminobenzidine (DAB) substrate−chromogen solution were purchased from DAKO (Carpinteria, CA).

2.2. Design and 3D Printing of the SSG and MSG. The MSG was designed using Inventor Professional (Autodesk, San Rafael, CA) and fabricated using an FDM 3D printer (Single Plus − 320C, Cubicon, Seongnam, Korea) with an acrylonitrile butadiene styrene (ABS) filament (Cubicon). After the 3D printing, it was post-treated with 100% acetone to smoothen the surface.[19] The MSG consists of four wings (1.5 × 2.5 × 1 mm^3, W × L × H), a center inlet (3 mm in diameter), and a side inlet (1.5−4 mm in diameter). The diameter of the side inlet was determined by the volume of solution (5−40 μL) to be added to the inlet (Figure 2A−E). The wings were designed to locate the MSG on 24-well plates (Corning, Corning, NY) (Figure 2F,G). The center and side inlets were connected by a channel (0.8 mm in height). The MSG can be reduced to fit into 96-well plates (Figure S1). The SSG, which had only the four wings and single center inlet, was fabricated in a similar way.

2.3. CFD Analysis. COMSOL Multiphysics version 5.5 (Burlington, MA) was used to perform CFD simulation to analyze the pattern of flow injected into the SSG and MSG. In both devices, flow was applied to the center inlet at 50 μL/s and analyzed for 1 s. The contact angle of the MSG was set at 60 or 120° for hydrophilic or hydrophobic MSG. Flow streamlines, pressure distributions, and forces were simulated at different flow rates (20−100 μL/s).

2.4. Measurement of the Maximum Cumulative Liquid Volume (MCLV) in the SSG and MSG. The MCLV was defined as the maximum addable volume without dropping hanging drops. The

https://doi.org/10.1021/acsami.3c02439
ACS Appl. Mater. Interfaces XXXX, XXX, XXX−XXX

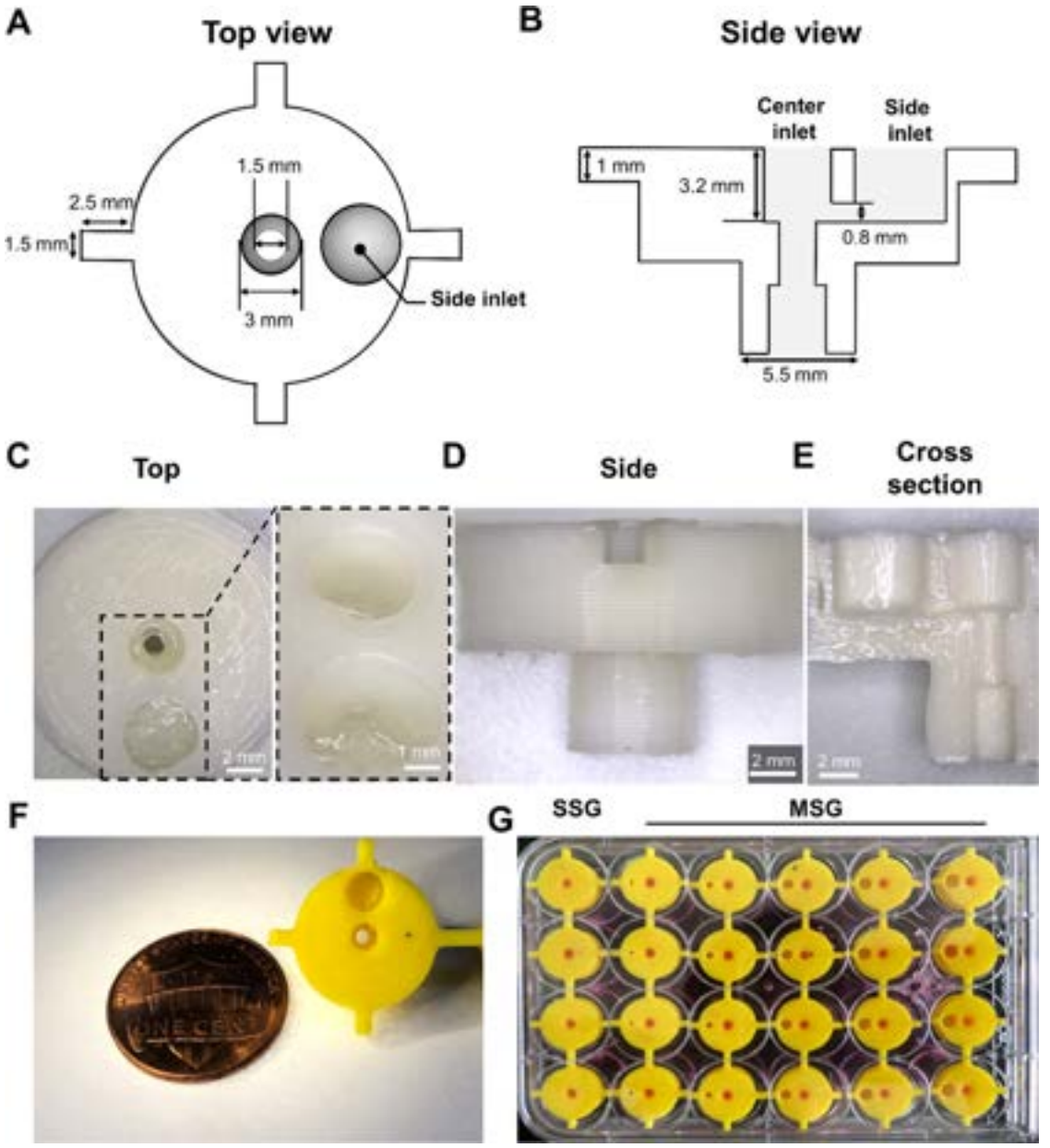

Figure 2. Design and fabrication of the MSG. (A) Top and (B) side views showing its dimensions. Real images of MSG showing (C) top, (D) side, and (E) cross-sectional views. (F) Stand-alone MSG and (G) arrays of the single-inlet spheroid generator (SSG) and MSG mounted on a 24-well plate.

MCLV of each device was measured to determine how much more liquid the MSG could hold compared to the SSG. For the measurement, both SSG and MSG were filled with 50 μL of phosphate-buffered saline (PBS; pH 7.4) containing green dye through the center inlet. Additional volumes (10−120 μL) of PBS were added into either the SSG through the center inlet or the MSG through the side inlet.

For comparing the flow movement of the additional solution entering the hanging drops, 50 μL of PBS was injected into the center inlet in SSG or MSG. Then, 40 μL of PBS with blue dye was injected into either the center inlet in SSG or the side inlet in MSG.

2.5. Cell Culture. The glioblastoma (GBM) cell line U87 and colon cancer cell line HT-29 were purchased from the American Type Culture Collection (Bethesda, MD). Patient-derived GBM cells (GBL28, GBL67, GBL15, GBL37, and GBL51) were obtained from the Brain Bank of Seoul National University Hospital (SNUH, Seoul, Korea). Their use was approved by the Institutional Review Board (IRB) of SNUH (H-0507-509-153). Human cancer-associated fibroblasts (CAFs) were obtained from Samsung Medical Center (SMC, Seoul, Korea) with IRB approval (SMC-2017-07-131-020). Mouse embryonic fibroblasts (MEFs) were provided by Dr. G.V. Shivashankar (National University of Singapore) and labeled with green fluorescent protein (GFP), as described previously.[20] Red fluorescent protein (RFP)-labeled U87 cells were purchased from Creative Biogene (Shirley, NY).

Wild-type U87, RFP-labeled U87, and patient-derived GBM cells were cultured in Petri dishes (100 mm in diameter, Corning) filled with MEM at 37 °C in a 5% CO_2 incubator. HT-29 cells and GFP-labeled MEFs were cultured in DMEM, and CAFs were cultured in MEM/F12. All media were supplemented with 10% (v/v) FBS, 100 units/ml penicillin, and 100 μg/mL streptomycin.

2.6. Spheroid Formation by the MSG. To inhibit cell adhesion in the MSG, 70 μL of 3% (w/v) BSA solution was added to the center and side inlets of the MSG, respectively, and incubated for 1 h at room temperature (RT). After incubation, the solution was removed by pipetting, and the MSG was washed with 200 μL of PBS. The

https://doi.org/10.1021/acsami.3c02439
ACS Appl. Mater. Interfaces XXXX, XXX, XXX−XXX

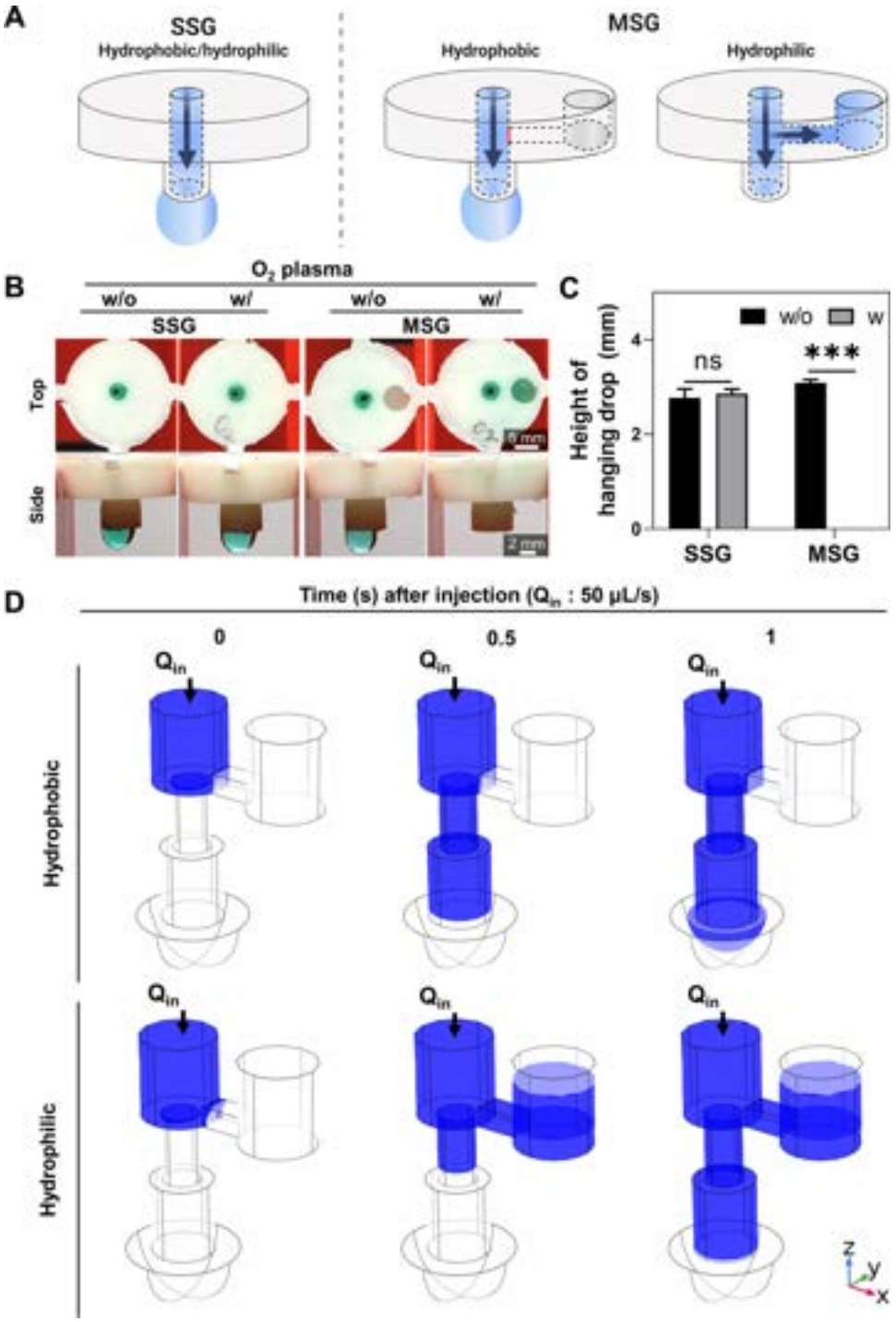

Figure 3. Effects of hydrophobicity and hydrophilicity on drop formation in the SSG and MSG. (A) Schematic describing the differential effects of hydrophilicity on hanging drop formation in the SSG and MSG. (B) Images of inlets (top view) and drops (side view) in the hydrophobic (without O_2 plasma treatment) and hydrophilic (with O_2 plasma treatment) SSGs and MSGs after injecting 60 μL of green ink through their center inlet. Hydrophobicity in the devices can be changed into hydrophilicity by O_2 plasma treatment at 100 W for 60 s using Cute (Femto Science, Hwaseong, Korea). (C) Height of drops in the hydrophobic and hydrophilic SSGs and MSGs. ***$p < 0.001$, two-tailed unpaired Student's t-test; ns, not significant ($n = 3$). (D) Computational fluid dynamics (CFD) simulation of flow patterns in the hydrophobic and hydrophilic MSGs over time. COMSOL Multiphysics version 5.5 was used for the simulation.

MSG was air-dried in a biosafety cabinet with ultraviolet light for 30 min.

Freshly prepared tumor cells were obtained from Petri dishes through trypsinization and suspended in their respective medium. Then, 1% (final conc.) methylcellulose was added to the cell suspensions to enhance cell aggregation.[21] A total of about 3000 cells were used to form a spheroid by loading 50 μL of each cell suspension (6×10^4 cells/mL) into the center inlet of the SSG or MSG. Both devices were incubated at 37 °C in 5% CO_2 for 2 days.[22]

2.7. Drug Treatment on Spheroids of Cell Line and PDCs in the MSG. Once U87 or GBL28 spheroids were formed in the MSG as described above, different volumes (0−40 μL) of 1 mM TMZ dissolved in DMSO were added to the MSG through the side inlet with different diameters (0−4 mm). The MSG was incubated at 37

https://doi.org/10.1021/acsami.3c02439
ACS Appl. Mater. Interfaces XXXX, XXX, XXX−XXX

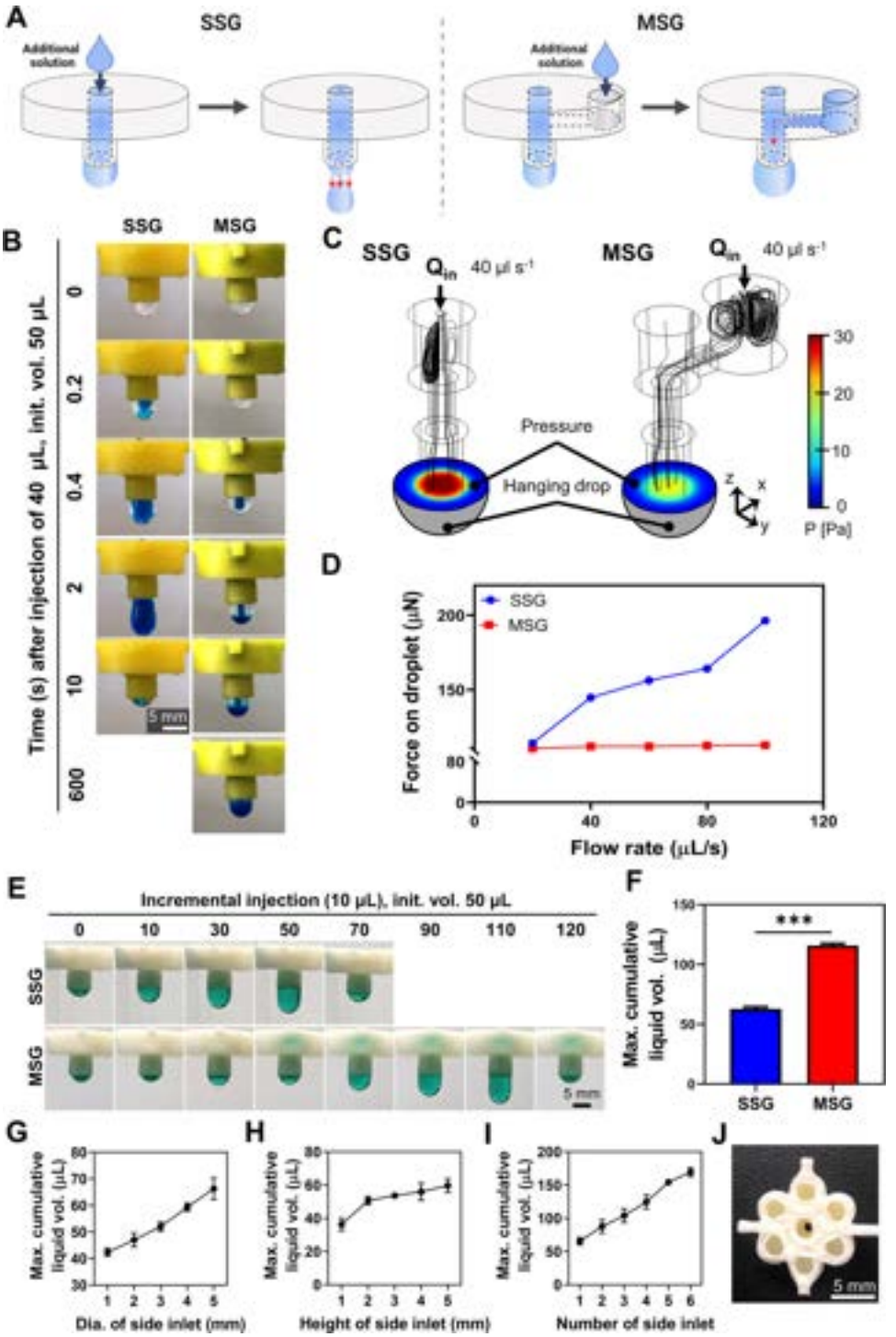

Figure 4. Liquid-holding capacity (LHC) of the SSG and MSG. (A) Schematic describing the behavior of hanging drops in the SSG and the MSG when an additional solution is injected through the center and side inlets, respectively. (B) Flow movement of an additional solution of 40 μL of PBS (blue) onto the hanging drops in the SSG and MSG previously formed by the injection of 50 μL of PBS (blank). Unlike the MSG, the SSG failed to hold the drop at 2 s after the additional injection through the center inlet. (C) CFD simulation of flow patterns in the SSG and MSG with the additional injection of 40 μL of PBS. Black lines represent the streamline injected from inlets. The color map represents the pressure distribution applied to the hanging drops. (D) Force applied to the hanging drops in the SSG and the MSG with the additional injection of 40 μL of PBS. (E) Images of hanging drops in the SSG and the MSG with the addition of different volumes (10 μL at a time) of solutions until hanging drops fall. (F) Maximum cumulative liquid volume (MCLV) in the SSG and the MSG. ***$p < 0.001$, two-tailed unpaired Student's t-test ($n = 4$). (G–I) MCLV of the MSG increases as the diameter (G), height (H), and number (I) of the side inlet increase. (J) An image of the MSG with six side inlets.

°C in a 5% CO_2 incubator for 2 days. After incubation, spheroids on the MSG were dropped into 24-well plates by flowing 50 μL of PBS into the center inlet and treated with a LIVE/DEAD Viability/ Cytotoxicity Kit. Bright-field and fluorescent images of spheroids were taken using a DeltaVision Elite Fluorescence microscope (GE Healthcare, Chicago, IL). These images were analyzed using ImageJ

https://doi.org/10.1021/acsami.3c02439
ACS Appl. Mater. Interfaces XXXX, XXX, XXX−XXX

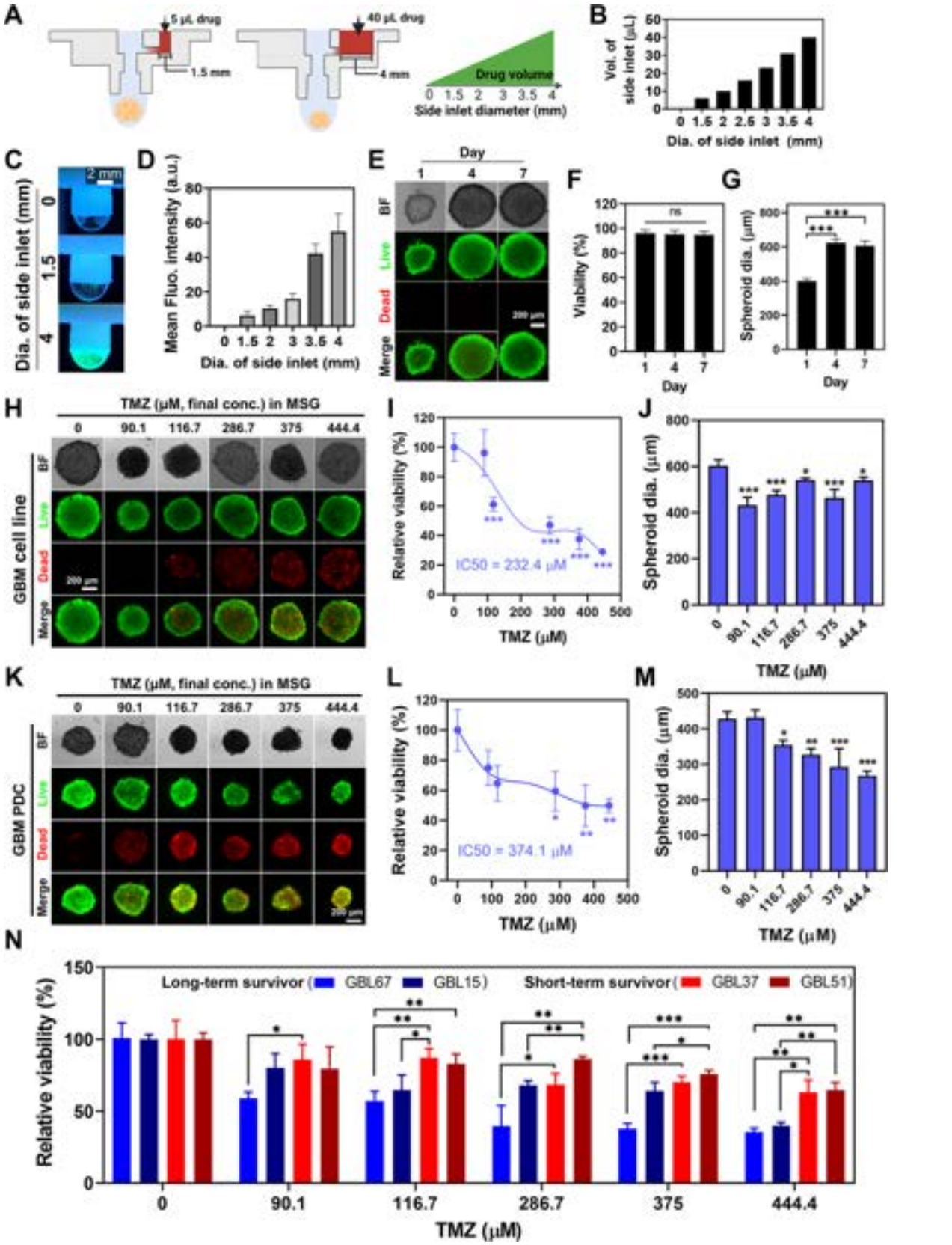

Figure 5. Simple HTS of drugs on tumor spheroids using the MSG having different diameters of side inlets. (A) Schematic diagram illustrating how to control drug concentration in hanging drops by changing the diameter of the side inlet. (B) Calculated volume that can be accommodated in a single side inlet with different diameters (0−4 mm). All side inlets are cylindrical and have the same height of 3.2 mm. (C) Images and (D) mean fluorescence intensities of hanging drops mixed with different volumes (0−40 μL) of an additional solution containing fluorescent particles injected through side inlets of different diameters (0−4 mm). (E) Bright-field (BF) and fluorescent images, (F) diameter, and (G) viability of spheroids of the U87 in hanging drops in the MSG with a diameter of 4 mm on different days (1−7). Live (green), calcein AM; dead (red), ethidium

https://doi.org/10.1021/acsami.3c02439
ACS Appl. Mater. Interfaces XXXX, XXX, XXX−XXX

Figure 5. continued

homodimer-1. (H−M) Viability and diameter of the glioblastoma (GBM) cell U87 (H−J) and patient cells GBL28 (K−M) spheroids on 2 days at different final temozolomide (TMZ) concentrations (0−444.4 μM), which was determined by injecting different volumes (0−40 μL) of 1 mM TMZ through the side inlets with different diameters (0−4 mm). Half-maximal inhibitory concentration (IC_{50}) of U87 = 232.4 μM, IC_{50} of GBL28 = 374.1 μM. Scale bar, 200 μm. Cell viability was calculated from the ratio of green fluorescence intensity to red fluorescence intensity. (N) Drug sensitivity assay of spheroids from long-term (GBL67 and GBL15; >2.5 years) and short-term survivors (GBL37 and GBL51; >1 year). *p < 0.05; **p < 0.01; ***p < 0.001, one-way ANOVA multiple comparison test; ns, not significant (n = 3).

(NIH, Bethesda, MD). Cell viability was calculated from the ratio of green fluorescence (calcein AM) intensity to red fluorescence (ethidium homodimer-1) intensity.[23] The viability of GBL67, GBL15, GBL37, and GBL51 spheroids was measured using the EZ-cytox Cell Viability Assay Kit according to the manufacturer's instructions.

For the combined drug treatment, the treatment sequence of ACNU and CDDP was changed on spheroids of MSG with three inlets. After spheroids were formed, 20 μL of 5 μM (final conc.) ACNU or CDDP was added in one side inlet and incubated for 24 h. After 24 h, 20 μL of 5 μM ACNU or CDDP was added to the other side inlets in the same manner and cultured for 24 h.

2.8. Formation of Single Spheroids with Different TSRs by the MSG. Spheroids with different TSRs (1:0−1:2) were obtained by adding 3,000 RFP-labeled U87 cells and different numbers (0−6,000 cells) of GFP-labeled MEFs into the center and side inlets on different days, respectively. In detail, single spheroids were first generated by loading 50 μL of RFP-labeled U87 suspension (6×10^4 cells/mL) through the center inlet and incubating them for 2 days in a 5% CO_2 incubator. Different numbers (0−6000 cells) of GFP-labeled MEFs were added to spheroids through the side inlet using a pipette. After that, spheroids with GFP-labeled MEFs in the MSG were incubated in a 5% CO_2 incubator for 24 h. Hanging drops in the MSG were dropped into 24-well plates and incubated again in a 5% CO_2 incubator for 7 days. To observe the spatial distribution of MEFs and tumor cells in spheroids, 3D images of spheroids were taken using a spinning-disk confocal microscope (Andor Dragonfly 302; Oxford Instruments, Concord, MA). To generate colon tumor spheroids with stroma-low (≤1:1) and stroma-high (>1:1) ratios, which are known as a prognostic cutoff value in colon cancer patients,[24] HT-29 spheroids on day 2 were mixed with different numbers (0−6000 cells) of CAFs through the side inlet. The mixture was incubated for 7 days in the CO_2 incubator until they were collected for histological and immunohistochemical studies.

2.9. Histology and Immunohistochemistry. Routine hematoxylin-and-eosin (H&E) staining protocol was used to stain the spheroid sections for histological examination.[25] HT-29 spheroids were fixed in 4% paraformaldehyde and embedded in 2% agarose. Agarose-embedded spheroids were fixed in 10% neutral buffered formalin for 12 h.

For immunohistochemical localization of Ki-67, a marker for cell proliferation, the sections in paraffin wax were deparaffinized in xylene, rehydrated in graded alcohol, and transferred to 0.01 M PBS. The sections were first incubated in EDTA (pH 9) for 3 min at 121 °C to reveal hidden antigen epitopes and later incubated with blocking solution for 20 min at RT. After blocking, they were incubated with anti-Ki-67 rabbit monoclonal antibody at 1:100 dilution at 4 °C overnight. The sections were washed with PBS (pH 7.4), and the remaining antibody was visualized using HRP-labeled polymer-conjugated secondary antibodies against rabbit IgG and ready-to-use DAB substrate−chromogen solution according to the manufacturer's instructions. Finally, the sections were lightly counter-stained with Mayer's hematoxylin for 20 s before dehydration and mounting.

2.10. Statistical Analysis. All data were represented as the mean ± standard deviation. Two-tailed unpaired Student's t-tests, one-way analysis of variance (ANOVA) multiple comparisons, and two-tailed unpaired multiple t-tests were used to compare the data groups. The levels of statistical significance were set as *p < 0.05, **p < 0.01, and ***p < 0.001. The number of samples was provided in the figure captions.

3. RESULTS

3.1. Hydrophobicity is Required for Hanging Drop Formation in the MSG. To understand the mechanism underlying how the MSG can hold large amounts of liquid, we investigated the effects of the surface hydrophobicity of the SSG and MSG on spheroid formation (Figure 3A). The water contact angle of the 3D printed ABS surface was measured to be approximately 113 degrees, indicating a hydrophobic surface.[26] The SSG has only one center inlet, whereas the MSG has a center inlet that produces a hanging drop and side inlets connected to the center inlet inside the chip. When the surface became hydrophilic by O_2 plasma treatment, the SSG could form water drops, while the MSG could not (Figures 3B,C and S2). This change can be explained by the fact that on the hydrophobic surface of the MSG, the injected fluid does not flow into the side inlet, but instead flows into the side inlet on the hydrophilic surface of the MSG (Figure 3B; Videos S1 and S2). This was further supported by the CFD simulation (Figure 3D; Videos S3 and S4). These results suggest that surface hydrophobicity is required for the MSG to form a hanging drop.

3.2. MSG Can Hold More Liquid Than SSG. The MSG can load an additional solution through the side inlet without increasing the force applied to the hanging drop (Figure 4A). When SSG and MSG previously filled with 50 μL of solution through the center inlet were injected with an additional 40 μL of solution through the center and side inlets, respectively, the drop hanging on SSG fell within 2 s, but the drop hanging on MSG did not. (Figure 4B). This can be explained by the CFD simulation showing that the fluid flows directly to the outlet of the SSG while changing the flow direction twice until it reaches the outlet of the MSG (Figure 4C). The pressure applied to the SSG drop was proportional to the flow rate, but that to the MSG was constant with increasing flow rate (Figure 4D). A similar trend was observed when additional solutions were incrementally injected into both devices (Figures 4E and S3). As a result, the MCLV of the MSG was significantly higher (p < 0.001) than that of the SSG (Figure 4F). The liquid-holding capacity (LHC) of the MSG can be further increased by increasing the diameter, height, and number of its side inlet (Figure 4G−I). In particular, more side inlets can increase the number of solutions that can be injected into the MSG. The MSG with multiple side inlets could be used to investigate the effect of drug combinations on a tumor spheroid as well as interactions of various types of stromal cells with cancer cells, which is required to recapitulate the TME.[2]

3.3. MSG for HTS. By changing the diameter of the side inlet, the final drug concentrations in the hanging drop on the MSG can be easily adjusted (Figure 5A). This is possible because the drug concentration in the MSG can be predetermined by the volume of the drug injected through

https://doi.org/10.1021/acsami.3c02439
ACS Appl. Mater. Interfaces XXXX, XXX, XXX−XXX

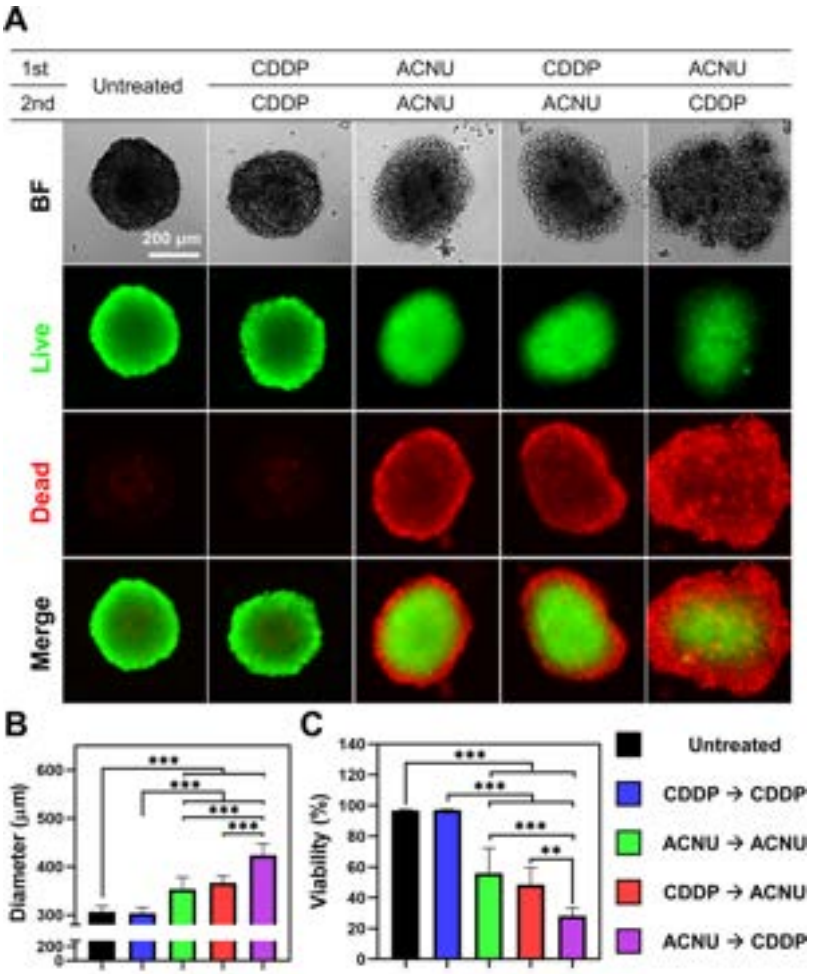

Figure 6. Combination drug therapy that controls the administration order of drugs in the MSG. (A) Live/dead staining images of U87 spheroids treated with 5 μM cisplatin (CDDP) or nimustine hydrochloride (ACNU) for 2 days with different orders by injecting them into different side inlets. Scale bar, 200 μm. (B) Diameter and (C) viabilities of U87 spheroids. $^{**}p < 0.01$; $^{***}p < 0.001$, one-way ANOVA multiple comparison test ($n = 3$).

the side inlet, which increases as the diameter of the side inlet increases. For example, when the cylindrical side inlet with a height of 3.2 mm has a diameter of 1.5, 2, 2.5, 3, 3.5, and 4 mm, respectively, its void volume is 5, 10, 20, 25, 30, and 40 μL (Figure 5B). This was demonstrated by observing an increase in the fluorescence intensity of the hanging drops when the side inlets of the same height (3.2 mm) but different diameters (0−4 mm) were filled with a solution containing the same concentration of fluorescent particles (Figure 5C,D). The amount of injection volume should be similar to that of the void volume of the side inlet; otherwise, the water level did not match that of the center inlet, and the flow went backward to the side inlet (Figure S4). Before drug treatment, it was confirmed that spheroids in the MSG increased their diameters and good viability of ~95% during the culture (1−7 days) (Figure 5E−G). Drug screening was demonstrated by treating spheroids of GBM cells (U87 and PDC) on the MSG having different diameters of side inlets with 1 mM TMZ (Figure 5H−M). When these spheroids were treated with various volumes (0, 5, 10, 20, 30, and 40 μL) of 1 mM TMZ that were equivalent to 0, 90.1, 166.7, 285.7, 375, and 444.4 μM, respectively (Supplementary Table S1), both spheroids showed a concentration-dependent cytotoxic effect. The half-maximal inhibitory concentration of TMZ on U87 and PDC spheroids was 232.4 and 374.1 μM, respectively.

The feasibility of the MSG for its application to HTS of the drug on patient samples was demonstrated by comparing the cytotoxic effects of TMZ on spheroids of GBM cells from either long-term survivors (GBL67 and GBL15) or short-term survivors (GBL37 and GBL51; Figure 5N). At 90.1 and 116.7 μM, there was statistical significance only between the survival rates of GBL67 and GBL37. However, when the concentration increased to 444.4 μM, it showed statistical significance between the survival rates of all long-term and short-term survivor spheroids. The survival rate of long-term survivor spheroids was <50%, whereas the survival rate of short-term survivor spheroids was >60%. This suggested that, when the patient was treated with the drug, the brain tumors of long-term survivors quickly killed cancer cells due to their high sensitivity to the drug, whereas short-term survivors were resistant to the drug, suggesting that cancer cells grew without being killed by the drug. The bioprinted GBM model also showed higher viabilities in short-term survivors than long-term survivors when treated with concurrent chemoradiation therapy.[27]

3.4. MSG for Combinatorial Drug Screening. In Figure 4J, it is shown that the MSG can be designed with upto six side

https://doi.org/10.1021/acsami.3c02439
ACS Appl. Mater. Interfaces XXXX, XXX, XXX−XXX

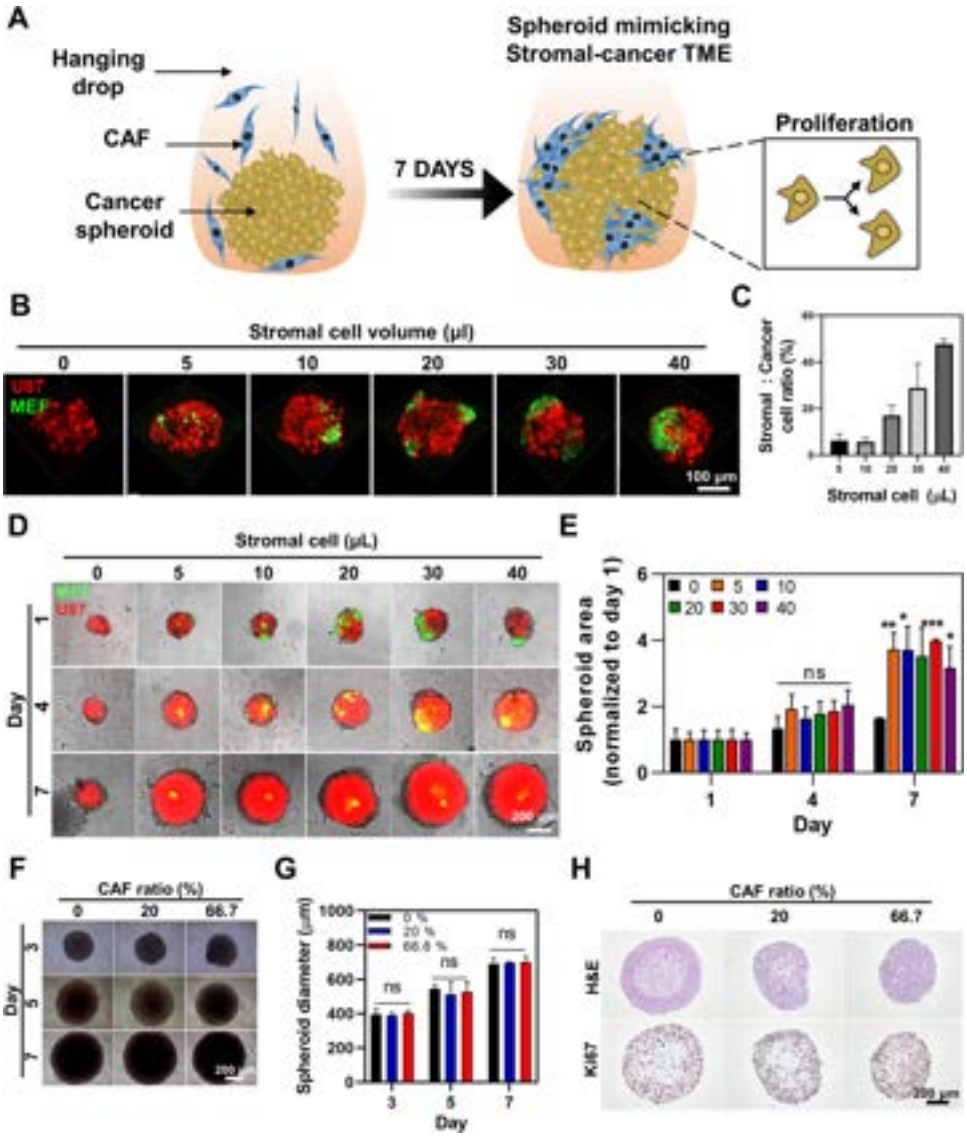

Figure 7. Effects of the tumor−stroma ratio (TSR) on tumor cell proliferation. (A) Schematic illustrating the MSG enabling the recapitulation of the TME in which tumor cells proliferate better through their interaction with cancer-associated fibroblasts (CAFs). (B) 3D confocal images of spheroids and (C) ratios of cancer cells to stroma cells in the tumor spheroids with different volumes of additional injection of mouse embryonic fibroblasts (MEFs). These spheroids were formed by the monoculture of an initially injected 3000 cells of U87 tumor cells labeled with red fluorescent protein (RFP) through the center inlet for 2 days, followed by the coculture of preformed U87 spheroids with additionally injected different volumes (0−40 μL) of MEFs labeled with green fluorescent protein (GFP) at 4.8×10^4 cells/mL through the side inlet for 1 day. Scale bar, 100 μm. The ratios were quantified by comparing the fluorescent intensity of GFP to that of RFP. (D) Fluorescent images and diameters (E) of tumor spheroids with different TSR ratios on different days (1−7) of coculture show the distribution of U87 (red) and MEF (green) cells. Scale bar, 200 μm. *$p < 0.05$; **$p < 0.01$; ***$p < 0.001$, Two-tailed unpaired Student's t-test. ns, not significant ($n = 3$). (F) Optical images, (G) diameter, and (H) H&E and Ki-67 images of the colon cancer line HT-29 spheroids with different CAF ratios (0−66.7%). Scale bar, 200 μm.

inlets, allowing for the addition of different drugs to a spheroid in the center inlet through each side inlet. This design feature enables the rapid assessment of synergistic effects in combinatorial treatments and the determination of treatment sequences for multiple drugs. To demonstrate the feasibility of this application, we chose to investigate the combination therapy of CDDP and ACNU. These drugs were selected based on studies showing high efficacy in patients with GBM.[28] U87 spheroids showed greater sensitivity in combination drug therapy than mono-drug therapy, and the sensitivity was also affected by the order (Figure 6A). U87 spheroids treated with only CDDP showed a viability of ∼95% and a diameter of ∼300 μm, similar to untreated spheroids (Figure 6B,C). Numerous dead cells were observed around the edge of spheroids that received ACNU treatment. These spheroids had a diameter of ∼350 μm, slightly larger than untreated spheroids. This increase might be related to apoptosis, which occurs on the periphery cells in the spheroids vulnerable to the drug reducing cell−cell adhesion.[29] The viability was significantly lower than when treated with CDDP. When CDDP and ACNU were treated together, it was confirmed that the sensitivity to drugs was significantly different according to the order of drug treatment. When ACNU was administered after CDDP, spheroid size and survival rate were similar to ACNU alone. However, when ACNU was administered first and CDDP was administered, spheroids loosened significantly,

https://doi.org/10.1021/acsami.3c02439
ACS Appl. Mater. Interfaces XXXX, XXX, XXX−XXX

the diameter increased to 400 μm, and the survival rate was 30%, showing the highest cytotoxicity against U87 spheroids.

3.5. Effects of TSRs on Spheroid Size and Cell Proliferation. The MSG can be used to modulate TSR, which plays a crucial role in tumor growth. TSRs were easily controlled in the tumor spheroids by injecting different volumes of stromal cells through the side inlets with different diameters (Figure 7A−C), similar to the way of drug treatment. On day 1 after injection of 5 and 10 μL of MEFs, they were spread in spheroids, whereas after injection of 20 μL and higher volumes of MEFs, they were concentrated in specific regions of spheroids (Figure 7B). The ratio between U87 cells and MEF was increased upto 50% when 40 μL of MEF was added into the side inlet (Figure 7C). On day 4, GFP-labeled MEFs moved to the center (Figure 7D). On day 7, spheroids with MEFs were larger than spheroids without MEFs but no differences between spheroids with different TSRs (Figure 7E).

The direct interaction of CAF and cancer cells was the principal factor for tumor proliferation. To closely mimic the TME, we used the colon cancer cell line HT-29 and their orthotopic CAFs. Similar to the result of U87 cells and MEFs, there were no significant effects of the CAF ratio on the diameter of tumor spheroids of HT-29 (Figure 7F,G). H&E staining showed that the core was less dense than the periphery when CAFs were not added (Figure 7H). However, the core became denser as the CAF ratio increased, indicating the penetration of CAFs into the tumor spheroids.[30] Ki-67 staining confirmed that spheroids with fibroblasts displayed much higher proliferation than spheroids without fibroblasts, which was also shown in the head and neck squamous cell carcinoma spheroids.[31]

4. DISCUSSION

The hanging drop method has been widely used to make tumor spheroids due to their simplicity of generation and reproducibility. Tumor spheroid production using the hanging drop method facilitates understanding the TME *in vivo* and HTS drug screening. However, the hanging drop method's main drawback is its limited capacity to handle large volumes of drugs or stromal cells for drug screening or stromal-cancer spheroid formation. This is due to the method's ability to hold only a drop of less than tens of microliters. To address this limitation, the MSG combines the hanging drop method with multiple inlets, greatly increasing its versatility. This approach offers several advantages.

First, the MSG enables the addition of solutions after spheroid formation without the risk of hanging drops falling, as shown in Figures 3 and 4. When additional solutions are added to the SSG, the hanging drops are susceptible to the forces applied by the fluid flow, resulting in their falling. The MSG's side inlets reduce the forces by approximately 0.58 times, preventing the hanging drops from falling and contributing to an increase in MCLV. The side inlets can hold designated volumes of additional liquids due to capillary force, enabling the MSG to retain larger volumes (Figure S5). Capillary forces cause liquid adhesion to the surfaces of the side inlet and pull the liquid, preventing it from flowing out. This is the first attempt to increase the stability of the hanging drop by lowering the pressure and increasing the MCLV during solution addition while taking advantage of the hanging drop method's ability to add a solution during spheroid culture.

Second, the MSG could easily control the volume of additional solutions by changing the diameters of the side inlets (Figure 5). MSG could be used to test the drug cytotoxicity on PDCs in an easy and high-throughput manner. Numerous microfluidic devices have been developed to conduct drug screening tests of tumor spheroids.[32] However, those devices need the fold dilution of drugs, which is inconvenient and requires many devices to do drug screening tests. In the MSG, the drug concentration can be determined by the volume of the drug injected through the side inlet, which is controlled by the diameter of the side inlet. Recently, the drug delivery system using a microcarrier has its advantage in improving the utilization rate by controlling the rate and amount of drug release and reducing the toxic side effects by maintaining the small and constant drug release.[33] Drugs incapsulated in microspheres, which can be an attractive option for treating a complicated tumor microenvironment can also be treated via side inlets of the MSG.[34] Similarly, spheroids with varied TSRs could be easily produced to observe their effects on the prognosis of cancer patients.[35] Conventionally, TSRs in spheroids were controlled by mixing each ratio manually.[5] The MSG can simply control the TSR by adding the stromal cells using side inlets with different diameters, making it easier and faster to produce different TSR spheroids (Figure 7). In the future, tri- or quad-cultures of various stromal cells are needed to be investigated because not only tumor-stromal cells but also stromal-immune cells have critical effects on the TME.[36] Especially in the GBM TME, microglia, the residual immune cells in the brain, promote cancer progression when interacting with tumor cells and show immunosuppressive potentials that make them difficult to be attacked by natural killer and T cells.[37]

At last, the injection order of solutions can be simply manipulated using multiple side inlets. Testing the efficacy of combination drug therapy is a good example of taking advantage of it (Figure 6). In cancer, it is necessary to treat a combination of various drugs because its capacity to cotarget various pathways gives a sensible therapeutic strategy for addressing the problem of drug resistance. For example, Thakuri et al. treated HT-29 spheroids with a combination of a drug candidate molecule and dactolisib and showed their strong synergistic effects.[38] Conventional hanging drop devices used in most drug screening methods typically involve mono-drug therapy, where the medium is removed from the center inlet and the drug is inserted. Conducting combination drug therapy using this method is difficult.[39] In contrast, the MSG's side inlets increase the number of solutions that can be injected into the device. The MSG makes it easy to investigate the efficacy of combination drug therapy, such as CDDP and ACNU, by controlling the order of drug administration through multiple side inlets without the hassle of removing the medium.

In summary, this study developed an MSG integrated with a 24-well plate. Using the MSG, drug screening and generation of different TSR spheroids could be conducted without losing spheroids. Drug testing controlled the volume of drugs injected into the side inlet, expanding conveniences by reducing experimental steps, such as drug dilution. Utilizing multiple side inlets, the effects of combination therapy with controlled order were determined. Furthermore, controlled TSR spheroids by the MSG mimicked a more clinically relevant TME, which could apply to the HTS test and to understand the cell-to-cell interactions of tumor and stromal cells by recapitulating

https://doi.org/10.1021/acsami.3c02439
ACS Appl. Mater. Interfaces XXXX, XXX, XXX−XXX

the patient's specific TME *in vivo*. In different TSR spheroids, TSR remarkably influenced the proliferation potential of the tumor, leading to different sizes and shapes of tumor spheroids.

5. CONCLUSIONS

The MSG is a highly versatile tool that enables the simple and stable injection of drugs and cells. The addition of side inlets greatly increases the volume of additional solutions that can be held and reduces the risk of hanging drops falling during the injection of additional solutions. The MSG has been successfully used for the screening of combination drugs as well as the recapitulation of the tumor microenvironment, suggesting its potential for a range of applications in drug development and cancer research.

In addition to drug screening and tumor spheroid formation, the MSG has several potential applications in chemical synthesis, reaction, assay, emulsion, and more. Its ability to add different solutions one by one opens up new possibilities for sequential chemical processes in a single drop. For example, the MSG could be used to create complex chemical reactions by adding different reagents in a specific order. The MSG could also be used to develop new assays for drug screening, such as adding a series of compounds to a spheroid to determine its response over time. In addition, the MSG could be used to create emulsions, which are important in a wide range of applications, including cosmetics, food production, and materials science. Furthermore, the MSG's potential for automation could greatly improve the efficiency of a range of chemical and biological processes, such as high-throughput drug screening and material synthesis. With further development, the MSG could become a valuable tool for both basic and applied research in a wide range of fields, including chemistry, biology, and materials science.

■ ASSOCIATED CONTENT

Supporting Information

The Supporting Information is available free of charge at https://pubs.acs.org/doi/10.1021/acsami.3c02439.

Table of final concentrations of TMZ in MSG; design of 96-well formatted MSG; measurement of water contact angle on the ABS treated w/ and w/o O_2 plasma; images of incremental injections of solutions into SSG or MSG; CFD results of MSG when the side inlet is not filled or filled; and images of MSG after injecting solutions into side inlet maintaining due to the capillary force (PDF)

Flows in MSG with O_2 plasma treatment (MP4)

Flows in MSG without O_2 plasma treatment (MP4)

CFD analysis for liquid flow in the hydrophobic MSG (MP4)

CFD analysis for liquid flow in the hydrophilic MSG (MP4)

■ AUTHOR INFORMATION

Corresponding Authors

Sun Ha Paek − *Department of Neurosurgery, Seoul National University Hospital (SNUH), Seoul 03080, Korea; Cancer Research Institute and Hypoxia Ischemia Disease Institute, Seoul National University Hospital (SNUH), Seoul 03080, Korea; Advanced Institute of Convergence Technology, Seoul National University (SNU), Suwon 16229, Korea*; Email: paeksh@snu.ac.kr

Sungsu Park − *School of Mechanical Engineering, Sungkyunkwan University (SKKU), Suwon 16419, Korea; Department of Biomedical Engineering and Department of Biophysics, Institute of Quantum Biophysics (IQB), Sungkyunkwan University (SKKU), Suwon 16419, Korea*; orcid.org/0000-0003-3062-1302; Phone: +82-31-290-7431; Email: nanopark@skku.edu

Authors

Seokgyu Han − *School of Mechanical Engineering, Sungkyunkwan University (SKKU), Suwon 16419, Korea*

Sein Kim − *Department of Biomedical Engineering, Sungkyunkwan University (SKKU), Suwon 16419, Korea*

Hye Kyung Hong − *Department of Surgery, Samsung Medical Center, School of Medicine, Seoul 06351, Korea*

Yong Beom Cho − *Department of Surgery, Samsung Medical Center, School of Medicine, Seoul 06351, Korea; Department of Health Sciences and Technology, SAIHST, Sungkyunkwan University (SKKU), Seoul 06351, Korea*

Hyo Eun Moon − *Department of Neurosurgery, Seoul National University Hospital (SNUH), Seoul 03080, Korea; Cancer Research Institute, Seoul National University Hospital (SNUH), Seoul 03080, Korea*

Complete contact information is available at: https://pubs.acs.org/10.1021/acsami.3c02439

Author Contributions

Conceptualization, S.H. and S.P.; methodology, S.H.; investigation, S.H. and H.G.H.; resources, H.G.H., Y.B.C., H.E.M., and S.H.P.; data curation, S.H.; writing—original draft preparation, S.H. and J.K.; writing—review and editing, Y.B. and S.H.P.; visualization, S.H. and H.G.H.; supervision, S.P.; project administration, S.P.; and funding acquisition, S.P. All authors have read and agreed to the published version of the manuscript.

Funding

This work was supported by the Technology Innovation Program (Industrial Strategic Technology Development Program−development of disease models based on 3D microenvironmental platforms mimicking multiple organs and evaluation of drug efficacy) (20008413) funded by the MOTIE (Ministry of Trade, Industry, and Energy) of Korea and the National Research Foundation of Korea (NRF) grant (No. RS-2023-00242443) funded by the MSIT (Ministry of Science and ICT) of Korea.

Notes

The authors declare no competing financial interest.

■ ACKNOWLEDGMENTS

The authors thank S. Kim at Samsung Medical Center for his valuable discussion.

■ REFERENCES

(1) Edmondson, R.; Broglie, J. J.; Adcock, A. F.; Yang, L. Three-dimensional Cell Culture Systems and their Applications in Drug Discovery and Cell-based Biosensors. *Assay Drug Dev. Technol.* **2014**, *12*, 207−218.

(2) Ellem, S. J.; De-Juan-Pardo, E. M.; Risbridger, G. P. In Vitro Modeling of the Prostate Cancer Microenvironment. *Adv. Drug Delivery Rev.* **2014**, *79*−*80*, 214−221.

(3) Asghar, W.; El Assal, R.; Shafiee, H.; Pitteri, S.; Paulmurugan, R.; Demirci, U. Engineering Cancer Microenvironments for In Vitro 3-D Tumor Models. *Mater. Today* **2015**, *18*, 539−553.

(4) Yeon, S.-E.; No, D. Y.; Lee, S.-H.; Lee, S. H.; Nam, S. W.; Nam, S. W.; Oh, I.-H.; Oh, I. H.; Lee, J.; Lee, J.; Kuh, H.-J. Application of Concave Microwells to Pancreatic Tumor Spheroids Enabling Anticancer Drug Evaluation in a Clinically Relevant Drug Resistance Model. *PLoS One* **2013**, *8*, No. e73345.
(5) Gupta, N.; Liu, J. R.; Patel, B.; Solomon, D. E.; Vaidya, B.; Gupta, V. Microfluidics-based 3D Cell Culture Models: Utility in Novel Drug Discovery and Delivery Research. *Bioeng. Transl. Med.* **2016**, *1*, 63−81.
(6) Yang, W.; Yu, H.; Li, G.; Wei, F.; Wang, Y.; Liu, L. Mask-free Fabrication of a Versatile Microwell Chip for Multidimensional Cellular Analysis and Drug Screening. *Lab Chip* **2017**, *17*, 4243−4252.
(7) Han, J.; Oh, S.; Hoang, H.-H.; Nguyen, D. T. T.; Lim, W.; Shin, T. H.; Lee, G.; Park, S. Recapitulation of Cancer Stem Cell Niches in Glioblastoma on 3D Microfluidic Cell Culture Devices under Gravity-driven Perfusion. *J. Ind. Eng. Chem.* **2018**, *62*, 352−361.
(8) Hasan, R. M. M.; Luo, X. Promising Lithography Techniques for Next-generation Logic Devices. *Nanomanuf. Metrol.* **2018**, *1*, 67−81.
(9) Lazar, A.; Mann, H. J.; Remmel, R. P.; Shatford, R. A.; Cerra, F. B.; Hu, W.-S. Extended Liver-specific Functions of Porcine Hepatocyte Spheroids Entrapped in Collagen Gel. *In Vitro Cell. Dev. Biol.: Anim.* **1995**, *31*, 340−346.
(10) Kelm, J. M.; Fussenegger, M. Microscale Tissue Engineering Using Gravity-enforced Cell Assembly. *Trends Biotechnol.* **2004**, *22*, 195−202.
(11) Nath, S.; Devi, G. R. Three-dimensional Culture Systems in Cancer Research: Focus on Tumor Spheroid Model. *Pharmacol. Ther.* **2016**, *163*, 94−108.
(12) Lin, R. Z.; Chang, H. Y. Recent Advances in Three-dimensional Multicellular Spheroid Culture for Biomedical Research. *Biotechnol. J.* **2008**, *3*, 1172−1184.
(13) Tung, Y. C.; Hsiao, A. Y.; Allen, S. G.; Torisawa, Y. S.; Ho, M.; Takayama, S. High-throughput 3D Spheroid Culture and Drug Testing Using a 384 Hanging Drop Array. *Analyst* **2011**, *136*, 473−478.
(14) Zhao, L.; Xiu, J.; Liu, Y.; Zhang, T.; Pan, W.; Zheng, X.; Zhang, X. A 3D Printed Hanging Drop Dripper for Tumor Spheroids Analysis without Recovery. *Sci. Rep.* **2019**, *9*, No. 19717.
(15) Lee, D. W.; Choi, Y.-S.; Seo, Y. J.; Lee, M.-Y.; Jeon, S. Y.; Ku, B.; Kim, S.; Yi, S. H.; Nam, D.-H. High-throughput Screening (HTS) of Anticancer Drug Efficacy on a Micropillar/Microwell Chip Platform. *Anal. Chem.* **2014**, *86*, 535−542.
(16) Du, G.-S.; Pan, J.-Z.; Zhao, S.-P.; Zhu, Y.; den Toonder, J. M.; Fang, Q. Cell-based Drug Combination Screening with a Microfluidic Droplet Array System. *Anal. Chem.* **2013**, *85*, 6740−6747.
(17) Li, X.; Fu, G.; Zhang, L.; Guan, R.; Tang, P.; Zhang, J.; Rao, X.; Chen, S.; Xu, X.; Zhou, Y.; et al. Assay Establishment and Validation of a High-throughput Organoid-based Drug Screening Platform. *Stem Cell Res. & Ther.* **2022**, *13*, 219.
(18) Fan, X.-y.; Deng, Z.-f.; Yan, Y.-y.; Orel, V. E.; Shypko, A.; Orel, V. B.; Ivanova, D.; Pilarsky, C.; Tang, J.; Chen, Z.-S. Application of Microfluidic Chips in Anticancer Drug Screening. *Bosn. J. of Basic Med. Sci.* **2021**, *22*, 302.
(19) Lalehpour, A.; Janeteas, C.; Barari, A. Surface Roughness of FDM Parts after Post-processing with Acetone Vapor Bath Smoothing Process. *J. Adv. Manuf. Technol.* **2018**, *95*, 1505−1520.
(20) Cui, Y.; Hameed, F. M.; Yang, B.; Lee, K.; Pan, C. Q.; Park, S.; Sheetz, M. Cyclic Stretching of Soft Substrates Induces Spreading and Growth. *Nat. Commun.* **2015**, *6*, No. 6333.
(21) Leung, B. M.; Lesher-Perez, S. C.; Matsuoka, T.; Moraes, C.; Takayama, S. Media Additives to Promote Spheroid Circularity and Compactness in Hanging Drop Platform. *Biomater. Sci.* **2015**, *3*, 336−344.
(22) Chen, Z.; Han, S.; Sanny, A.; Chan, D. L.-K.; van Noort, D.; Lim, W.; Tan, A. H.-M.; Park, S. 3D Hanging Spheroid Plate for High-throughput CAR T Cell Cytotoxicity Assay. *J. Nanobiotechnol.* **2022**, *20*, 30.
(23) Lim, W.; Park, S. A Microfluidic Spheroid Culture Device with a Concentration Gradient Generator for High-throughput Screening of Drug Efficacy. *Molecules* **2018**, *23*, 3355.
(24) Van Pelt, G. W.; Sandberg, T. P.; Morreau, H.; Gelderblom, H.; van Krieken, J. H. J.; Tollenaar, R. A.; Mesker, W. E. The tumour−stroma Ratio in Colon Cancer: the Biological Role and its Prognostic Impact. *Histopathology* **2018**, *73*, 197−206.
(25) Gamble, M.; Wilson, I. The Hematoxylins and Eosin. In *Theory and Practice of Histological Techniques*, 6th ed.; Elviser, 2008; pp 121−134.
(26) Tsougeni, K.; Vourdas, N.; Tserepi, A.; Gogolides, E.; Cardinaud, C. Mechanisms of Oxygen Plasma Nanotexturing of Organic Polymer Surfaces: from Stable Super Hydrophilic to Super Hydrophobic Surfaces. *Langmuir* **2009**, *25*, 11748−11759.
(27) Yi, H.-G.; Jeong, Y. H.; Kim, Y.; Choi, Y.-J.; Moon, H. E.; Park, S. H.; Kang, K. S.; Bae, M.; Jang, J.; Youn, H.; et al. A Bioprinted Human-glioblastoma-on-a-chip for the Identification of Patient-specific Responses to Chemoradiotherapy. *Nat. Biomed. Eng.* **2019**, *3*, 509−519.
(28) Kim, I. H.; Park, C.-K.; Heo, D. S.; Kim, C.-Y.; Rhee, C. H.; Nam, D.-H.; Lee, S. H.; Han, J. H.; Lee, S.-H.; Kim, T. M.; et al. Radiotherapy Followed by Adjuvant Temozolomide with or without Neoadjuvant ACNU-CDDP Chemotherapy in Newly Diagnosed Glioblastomas: a Prospective Randomized Controlled Multicenter Phase III Trial. *J. Neuro-Oncol.* **2011**, *103*, 595−602.
(29) Mittler, F.; Obeïd, P.; Rulina, A. V.; Haguet, V.; Gidrol, X.; Balakirev, M. Y. High-content Monitoring of Drug Effects in a 3D Spheroid Model. *Front. Oncol.* **2017**, *7*, 293.
(30) Madar, S.; Goldstein, I.; Rotter, V. 'Cancer Associated fibroblasts'−More Than Neets the Eye. *Trends Mol. Med.* **2013**, *19*, 447−453.
(31) Magan, M.; Wiechec, E.; Roberg, K. CAFs Cffect the Proliferation and Treatment Response of Head and Neck Cancer Spheroids during Co-culturing in a Unique In Vitro Model. *Cancer Cell Int.* **2020**, *20*, 1−11.
(32) Chen, Y.; Gao, D.; Liu, H.; Lin, S.; Jiang, Y. Drug Cytotoxicity and Signaling Pathway Analysis with Three-dimensional Tumor Spheroids in a Microwell-based Microfluidic Chip for Drug Screening. *Anal. Chim. Acta* **2015**, *898*, 85−92.
(33) Ekanem, E. E.; Nabavi, S. A.; Vladisavljević, G. T.; Gu, S. Structured Diodegradable Polymeric Microparticles for Drug Delivery Produced Using Flow Focusing Glass Microfluidic Devices. *ACS Appl. Mater. Interfaces* **2015**, *7*, 23132−23143.
(34) Huang, P.; Wang, X.; Liang, X.; Yang, J.; Zhang, C.; Kong, D.; Wang, W. Nano-, Micro-, and Macroscale Drug Delivery Systems for Cancer Immunotherapy. *Acta Biomater.* **2019**, *85*, 1−26.
(35) Chen, Y.; Zhang, L.; Liu, W.; Liu, X. Prognostic Significance of the Tumor-stroma Ratio in Epithelial Ovarian Cancer. *Biomed Res. Int.* **2015**, *2015*, 1−8.
(36) Xi, K.-X.; Wen, Y.-S.; Zhu, C.-M.; Yu, X.-Y.; Qin, R.-Q.; Zhang, X.-W.; Lin, Y.-B.; Rong, T.-H.; Wang, W.-D.; Chen, Y.-Q.; Zhang, L. J. Tumor-stroma Ratio (TSR) in Non-small Cell Lung Cancer (NSCLC) Patients after Lung Resection is a Prognostic Factor for Survival. *J. Thorac. Dis.* **2017**, *9*, 4017.
(37) Roesch, S.; Rapp, C.; Dettling, S.; Herold-Mende, C. When Immune Cells Turn Bad—Tumor-associated Microglia/Macrophages in Glioma. *Int. J. Mol. Sci.* **2018**, *19*, 436.
(38) Shahi Thakuri, P.; Tavana, H. Single and Combination Drug Screening with Aqueous Biphasic Tumor Spheroids. *SLAS Discovery* **2017**, *22*, 507−515.
(39) Carvalho, M. R.; Lima, D.; Reis, R. L.; Oliveira, J. M.; Correlo, V. M. Anti-cancer Drug Validation: The Contribution of Tissue Engineered Models. *Stem Cell Rev. Rep.* **2017**, *13*, 347−363.

https://doi.org/10.1021/acsami.3c02439
ACS Appl. Mater. Interfaces XXXX, XXX, XXX−XXX